Hexamethylenetetramine Directed Synthesis and Properties of a New Family of α-Nickel Hydroxide Organic−Inorganic Hybrid Materials with High Chemical Stability

Bian-Hua Liu, Shu-Hong Yu,* Shao-Feng Chen, and Chun-Yan Wu

Division of Nanomaterials and Chemistry, Hefei National Laboratory for Physical Sciences at Microscale, Structure Research Laboratory of CAS, School of Chemistry and Materials, University of Science and Technology of China, Hefei 230026, P. R. China

Received: October 19, 2005; In Final Form: December 13, 2005

A new family of organic−inorganic hybrid material of α-nickel hydroxide formulated as $Ni(OH)_{2-x}(A^{n-})_{x/n}$-$(C_6H_{12}N_4)_y \cdot zH_2O$ ($A = Cl^-$, CH_3COO^-, SO_4^{2-}, NO_3^-; $x = 0.05-0.18$, $y = 0.09-0.11$, $z = 0.36-0.43$) with high stability and adjustable interlayer spacing ranging from 7.21 to 15.12 Å has been successfully prepared by a simple hydrothermal method. The effects of various anions and hexamethylenetetramine (HMT) on the *d* values of α-nickel hydroxide have been systematically investigated. This family of hybrid materials is of such high stability that they can stand more than 40 days in 6 M KOH. The product with a formula $Ni(OH)_{1.95}(C_6H_{12}N_4)_{0.11}(Cl^-)_{0.05}(H_2O)_{0.36}$ has a high surface area of about 299.26 m^2/g and an average pore diameter of about 45.1 Å. The coercivity (*Hc*) value is ca. 2000 Oe for the sample with a *d* spacing of 13.14 Å. Moreover, the prepared α-$Ni(OH)_2$ in our experiment is of high stability in strong alkali solution. Such high stability could be derived from strong chelating interactions between the Ni ions and HMT molecules with the interlayers. This high chemical stability could make this material more suitable for the applications.

Introduction

Layered double hydroxides (LDHs) are important lamellar materials,[1] which can be structurally characterized as containing brucite-like (magnesium hydroxide like) layers in which some divalent metal cations are substituted by trivalent ions to form positively charged sheets.[2] The metal cations occupy the centers of octahedra whose vertexes contain hydroxide ion. By sharing octahedral edges, these octahedra are connected to each other to form an infinite sheet. Also, the residual positive charge in the layers is compensated for by the presence of hydrated anions between the stacked sheets.[3] On the basis of their wide applications in the production of catalyst, sorbents, ionic exchangers, ionic conductors and electrochemical materials,[4] layered hydroxide materials have attracted a lot of interest in recent years.[5]

Nickel hydroxide ($Ni(OH)_2$) as a typical LDH, has important applications in alkaline rechargeable batteries such as Ni−Cd, Ni−Zn, Ni−Fe, and Ni−MH storage batteries,[6] and also as a precursor for catalysts and NiO.[7,8] There exist two polymorphs of nickel hydroxide, α- and *β*-phases.[9] Both forms crystallize in the hexagonal system with the brucite-type structure by stacking $Ni(OH)_2$ layers along the *c*-axis. The main difference between α- and *β*-$Ni(OH)_2$ phase is if there exist other ions or molecules between the stacking layers along the *c*-axis. α-Nickel hydroxide consists of stacked $Ni(OH)_{2-x}$ layers intercalated with various anions[10] (e.g., carbonate, nitrate, etc.) or water molecules in the interlayer space to maintain charge neutrality totally.[11] Hydrotalcite is a natural mineral $Mg_6Al_2(OH)_{16}CO_3 \cdot 4H_2O$, which both Mg^{2+} and Al^{3+} are located in brucite ($Mg(OH)_2$) type sheets while CO^{3-} anions occupy the intersheet space to balance extra positive charges carried by trivalent Al^{3+} cations (compared to divalent Mg^{2+}).[12] In fact, besides being an isomorph of LDHs, α-nickel hydroxide is also isostructural with hydrotalcite-like (HT-like) compounds.[13] However, *β*-$Ni(OH)_2$ is of brucite-like ($Mg(OH)_2$) structure but without intercalated species. Nevertheless, the $Ni(OH)_2$ layer of two polymorphs consists of a hexagonal planar arrangement of octahedrally oxygen-coordinated Ni(II) ions in the same way.

For the *β*-$Ni(OH)_2$, layers are perfectly stacked along the *c*-axis with an interlamellar distance of 4.6 Å; while for the α-$Ni(OH)_2$, layers are completely misoriented relative to each other, corresponding to a so-called turbostratic phase with the presence of water molecules and anionic species in the van der Waals gap.[14] The interlamellar distance of the layers of α-Ni-$(OH)_2$ is about 7.5 Å. However, *d* spacing of the interlayers can be adjusted from 7.5 to 31.7 Å [2,10] while long carbon chain organic molecules ($C_nH_{2n+1}SO_3^-$, $n = 10, 12, 14, 18$) were imposed into the interlayer of α-$Ni(OH)_2$ to form Ni-$(C_nH_{2n+1}SO_3^-)_x(OH)_{2-x} \cdot yH_2O$. Comparing with *β*-$Ni(OH)_2$, α-$Ni(OH)_2$ has better electrochemical properties but less stability.[15,16] To improve its stability, researchers have mingled some metal cations (Al^{3+},[17,18] Zn^{2+},[19] and Co^{3+} [20]) into the α-phase to form a hydrotalcite-like compound formulated as $Ni_{1-x}Al_x$-$(OH)_2(CO_3^{2-})_{2/x} \cdot nH_2O$.[12b,21]

In this report, we present a convenient method to obtain new and stable turbostratic α-$Ni(OH)_2$ organic−inorganic hybrid material with adjustable *d* spacing by introducing different anions and hexamethyltetramine (HMT). The interlayer spacing of the α-$Ni(OH)_2$ varies, depending on the inserted anion species and the amount of HMT. The molecular structure of the α-nickel hydroxide can be formulated as $Ni(OH)_{2-x}(A^{n-})_{x/n}$-$(C_6H_{12}N_4)_y \cdot zH_2O$ ($A = Cl^-$, CH_3COO^-, SO_4^{2-}, NO_3^-; $x = 0.05-0.18$, $y = 0.09-0.11$, $z = 0.36-0.43$) with different interlayer *d* spacing ranging from 7.21 to 15.12 Å. Importantly, as-synthesized α- $Ni(OH)_2$ is highly stable in strong alkali or acidic solution compared with that reported previously. After heat treatment at 600 °C in the air atmosphere, the α-nickel

* To whom correspondence should be addressed. Fax: + 86 551 3603040, E-mail: shyu@ustc.edu.cn.

10.1021/jp055970t CCC: $33.50
Published on Web 02/14/2006

TABLE 1: Summary of the Main Results on the *d* Spacings of the Products Obtained under Different Reactant Concentrations, Where d_t Is the Typical Diffraction Peak and d_f Is the First Diffraction Peak

no.	nickel source (1 mmol)	dosage of HMT (mmol)	salts		d_t (Å)	d_f (Å)
			species	dosage (mmol)		
A1	$Ni(Ac)_2$	10	NaAc	10	8.14	12.88
A2	$Ni(Ac)_2$	10	NaAc	20	8.31	14.20
A3	$Ni(Ac)_2$	20	NaAc	10	8.10	15.12
A4	$Ni(Ac)_2$	20	NaAc	20	8.31	14.67
B1	$NiCl_2$	10	NaCl	10	8.39	13.26
B2	$NiCl_2$	10	NaCl	20	8.70	12.99
B3	$NiCl_2$	20	NaCl	10	8.02	12.48
B4	$NiCl_2$	20	NaCl	20	8.77	12.91
C1	$Ni(NO_3)_2$	10	$NaNO_3$	10	7.21	13.71
C2	$Ni(NO_3)_2$	10	$NaNO_3$	20	8.48	14.48
C3	$Ni(NO_3)_2$	20	$NaNO_3$	10	7.25	13.22
C4	$Ni(NO_3)_2$	20	$NaNO_3$	20	8.10	13.35
D1	$NiSO_4$	10	Na_2SO_4	10	8.94	13.88
D2	$NiSO_4$	10	Na_2SO_4	20	9.02	13.50
D3	$NiSO_4$	20	Na_2SO_4	10	8.89	13.70
D4	$NiSO_4$	20	Na_2SO_4	20	9.04	13.30

hydroxide can completely transform into nickel oxide (NiO). The magnetic properties and the porosities of the samples have been also investigated.

Experimental Section

Chemicals. All chemicals were analytical grade and purchased from Shanghai Chemical Reagents Company. These chemicals are hexamethylenetetramine (HMT, $C_6H_{12}N_4$, M_w = 140.19), nickel acetate ($Ni(AC)_2 \cdot 4H_2O$, M_w = 248.86), nickel chloride ($NiCl_2 \cdot 6H_2O$, M_w = 237.69), nickel nitrate ($Ni(NO_3)_2 \cdot 6H_2O$, M_w = 290.80), nickel sulfate ($NiSO_4 \cdot 6H_2O$, M_w = 262.83), sodium acetate (NaAc, M_w = 82.03), sodium chloride (NaCl, M_w = 58.44), sodium nitrate ($NaNO_3$, M_w = 84.89), and sodium sulfate (Na_2SO_4, M_w = 142.42). All reagents were used without further purification.

Synthesis Procedures. In a typical experiment, 1 mmol of nickel acetate ($Ni(AC)_2 \cdot 4H_2O$), 10 mmol of HMT, and 10 mmol of sodium acetate were added into 40 mL of deionized water with stirring until the solution was clear. Then, the solution was put into a 50 mL capacity Teflon-lined autoclave. After being sealed, the autoclave was heated at 140 °C for 10 h. After hydrothermal treatment, green or pale blue precipitate was separated from the solution by centrifugation, washed with deionized water and absolute ethanol for several times, and dried at 60 °C for 4 h in a vacuum. To understand the effects of anions on the formation of α-nickel hydroxide, nickel chloride (with sodium chloride), nickel sulfate (with sodium sulfate), and nickel nitrate (with sodium nitrate) were used in equal molar amounts to substitute for the nickel acetate (see details in Table 1).

Chemical Stability. The chemical stability of the synthesized α-nickel hydroxide samples was examined by immersing the powders in 6 M HNO_3 and 6 M and 12 M KOH solutions for a long time. After immersion, the products were collected by centrifugation, then washed by deioned water and absolute ethanol, and finally, dried at 60 °C for 4 h in a vacuum for powder X-ray diffraction measurement.

Characterization. The products were characterized by X-ray diffraction pattern (XRD), recorded on a MAC Science Co. Ltd. MXP 18 AHF X-ray diffractometer with monochromatized Cu Kα radiation (λ = 1.54056 Å). Transmission electron microscopy (TEM) and high-resolution transmission electron microscopy (HRTEM) were performed on a Hitachi (Tokyo, Japan) H-800 transmission electron microscope (TEM) at an accelerating voltage of 200 kV and a JEOL-2010 high-resolution transmission electron microscopy (HRTEM), also at 200 kV, respectively. SEM images were taken on a JEOL JSM-6700F scanning electron microscope; the infrared spectrum was obtained on a Fourier transform infrared spectrometer (FRIR, Magna-IR-750); thermogravimetric analysis (TGA) was carried out on a TGA-50 thermal analyzer (Shimadzu Corporation) with a heating rate of 10 °C min^{-1} in flowing air. Element analysis was carried out on an INCA300 X-ray Energy Spectrum instrument (OXFORD). N_2 adsorption was determined by BET measurements using an ASAP-2000 surface area analyzer. The magnetic measurements on powdered samples enclosed in a medical cap were carried out at 4 K using a commercial SQUID magnetometer (MPMS-XL) from Quantum Design Corp.

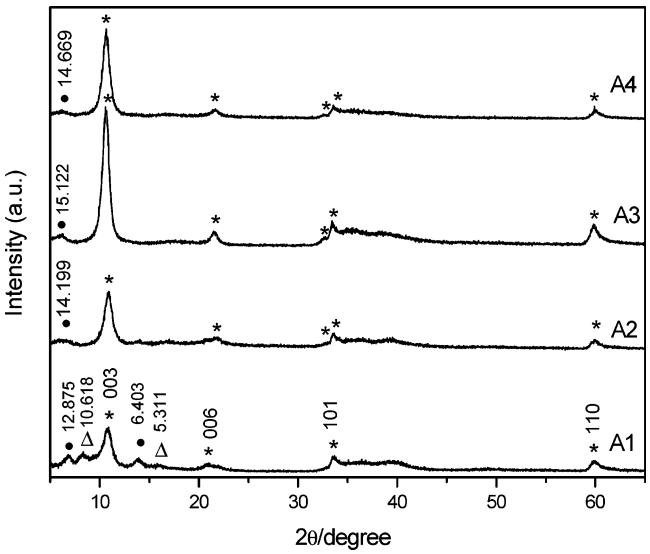

Figure 1. XRD patterns of α-$Ni(OH)_2$ samples obtained at 140 °C for 10 h when $Ni(Ac)_2 \cdot 4H_2O$ was selected as nickel source. The initial amount of reactants for the samples are respectively: sample A1, 1 mmol $Ni(Ac)_2 \cdot 4H_2O$ + 10 mmol HMT + 10 mmol NaAc; sample A2, 1 mmol $Ni(Ac)_2 \cdot 4H_2O$ + 10 mmol HMT + 20 mmol NaAc; sample A3, 1 mmol $Ni(Ac)_2 \cdot 4H_2O$ + 20 mmol HMT + 10 mmol NaAc; sample A4, 1 mmol $Ni(Ac)_2 \cdot 4H_2O$ + 20 mmol HMT + 20 mmol NaAc (see details in Table 1). The peaks labeled with an asterisk can be indexed to the typical diffraction of α-$Ni(OH)_2$. The peaks labeled with ● and △ may be indexed to the new series of *d* spacings between interlayers of α-$Ni(OH)_2$ (see details in text).

Results and Discussion

Synthesis of α-$Ni(OH)_2$ Organic—Inorganic Hybrid Materials. Previously, the XRD pattern of α-$Ni(OH)_2$[13,22−24] presented a series of typical peaks with a low angle reflection around 7.79 Å, secondary reflections at 3.90 and 1.54 Å, and a broad asymmetric band at 2.2−2.7 Å. Figure 1 shows the XRD patterns of as-prepared products with the same amount of nickel acetate at different amount of HMT and sodium acetate via the hydrothermal treatment at 140 °C for 10 h. All of the XRD patterns (samples A1−A4) have the characteristic diffraction peaks of α-$Ni(OH)_2$ and show a diffraction peak at low angle (2θ located at about 10°) around 8.10−8.30 Å and a broad asymmetric band at about 2.66 Å. The asymmetric nature of the reflection at about d = 2.66 Å indicates the formation of a turbostratic phase observed in most of the α-type hydroxides, corresponding to the formation of α-form of nickel hydroxide.[25]

From Figure A1 (see the experiment details in Table 1), the entire asterisk labeled peaks obviously display hydrotalcite-like features[26,27] and the *d* values at 8.14, 4.05, 2.66, and 1.54 Å could also be assigned to (003), (006), (101), and (110) planes

of α-Ni(OH)$_2$. The characteristic XRD pattern of hydrotalcite-like structures is that the d values are corresponding to successive diffraction peaks by basal planes; i.e., $d_{003} \approx 2d_{006} \approx 3d_{009}$. The value of $d(00l)$ depends on the thickness of the brucite-like layer and on the nature of the interlayer anions.[25]

Furthermore, the d values of the samples corresponding to successive diffractions by the basal planes agree well with each other, i.e., $d_{003} \approx 2d_{006}$. According to the literature,[26,28] the cell constant c is commonly calculated as $c = 3d_{003}$, assuming a 3R polytipism for the hydrotalcite, while the value of cell constant a is calculated as $a = 2d_{110}$.[12a] It has been also proposed that c can be better determined by averaging the position to the (003), (006), and (009) planes[29] according to eqs 1 and 2:

$$c/3 = 1/2(d(003) + (2d(006))) \quad (1)$$

$$c/3 = 1/3(d(003) + (2d(006) + (3d(009)))) \quad (2)$$

On the basis of the d spacing of the reflections in the XRD pattern of the sample A1 in Figure 1, we can calculate the cell parameters of the sample A1 as $a = 3.08$ Å and $c = 24.91$ Å, and the calculated c value is larger than those reported earlier for α-Ni(OH)$_2$ particles precipitated from urea-containing solutions.[30,31] The d_{003} spacing of the products obtained here is about 8.10 Å, which is larger than the d spacing of the literature value 7.79 Å (JCPDS Card 38-0715). It is well-known that the main feature of α-nickel hydroxide is that Ni(OH)$_2$ layers could be intercalated with various anions.[10] So, such a spacing difference may correspond to the difference in the thickness of a poorly packed molecule layer separating the octahedral Ni(OH)$_2$ sheets or the amount of the anion(CH_3COO^-) intercalated to the Ni(OH)$_2$ layers.[32,33] In fact, the previous literature reported that intercalation of a large amount of water[21a] and other anions[2] to the interlayers of α-Ni(OH)$_2$ can also influence the value of the d spacings.

Furthermore, we also found that new series peaks have occurred in the XRD pattern for sample A1 in Figure 1. Here the peaks labeled with dots correspond to $d_1 = 12.8750$ Å and $d_2 = 6.4025$ Å which have a characteristic of $d_1 \approx 2d_2$ (12.8750 Å ≈ 2 × 6.4025 Å), and the same is true for the peaks labeled with triangles (10.6180 Å ≈ 2 × 5.3107 Å). From above calculated c values ($c = 24.91$ Å), it can be seen that $d_1 \approx 1/2c$, $d_2 \approx 1/4c$. These two peaks can be indexed to the diffraction of $d(002)$ and $d(004)$ of α-Ni(OH)$_2$. The peaks labeled with triangles (10.6180 Å ≈ 2 × 5.3107 Å) can also be treated as the new diffraction of α-Ni(OH)$_2$ due to the disorder property of the layered double hydroxide (hydrotalcite-like features).[26,27] When the amounts of HMT and sodium acetate are varied, the XRD patterns of these samples also present typical peaks for α-Ni(OH)$_2$, but the d value of the first peak ranges from 12.87 to 15.12 Å. This phenomenon may be induced by the extent of intercalating organic molecules in the layered structure of the α-Ni(OH)$_2$.[22a,34] No peaks for β-Ni(OH)$_2$ can be observed in these XRD patterns shown in Figures 1 and 2.

To study the effect of anions on the final products, acetate anion was replaced by chloride, nitrate and sulfate anions, respectively. The summary of experimental details is listed in Table 1. The XRD patterns (Figure 2) presented a typical hydrotalcite-like structure just like the patterns shown in Figure 1. Each XRD pattern shown in Figure 2 presents a series of typical peaks and a broad of asymmetric band (labeled by dot lines), which can be characterized as α-Ni(OH)$_2$. Moreover, other peaks labeled with asterisk also show the hydrotalcite-like structure feature, which can be treated similarly as stated above. From Table 1 and Figure 2, interesting information can

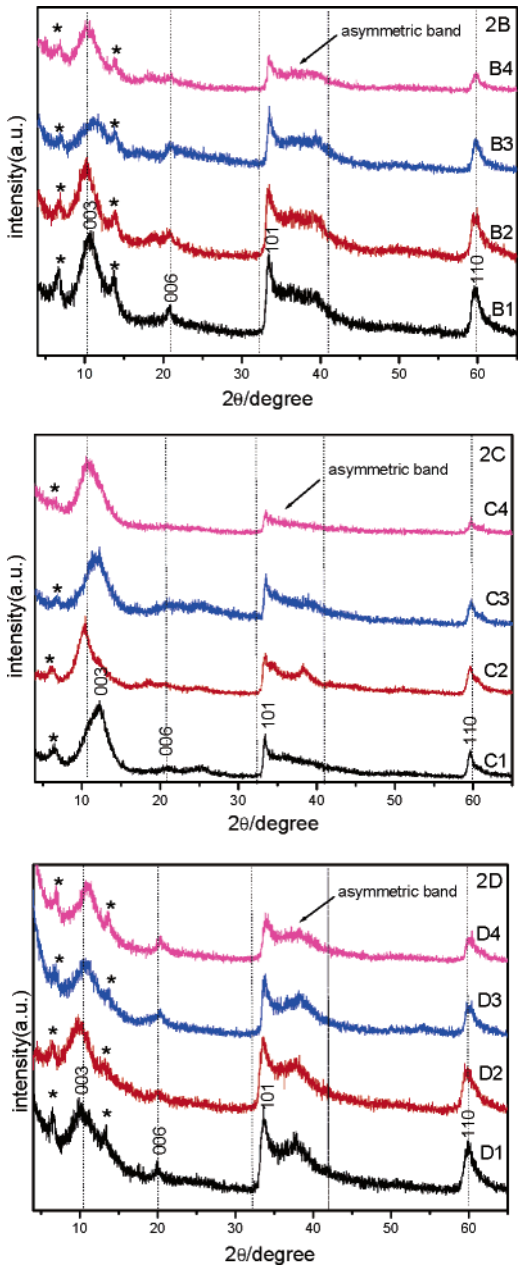

Figure 2. XRD patterns of α-Ni(OH)$_2$ samples obtained with different nickel sources and corresponding sodium salts. The 2B sample series B1−B4 correspond to the products obtained using nickel chloride as nickel source; the 2C sample series correspond to the products obtained using nickel nitrate as nickel source; the 2D sample series correspond to the products obtained using nickel sulfate as nickel source. The compositions of all these samples are shown in Table 1. The peaks labeled with the dot line can be assigned as the typical reflection of α-Ni(OH)$_2$, labeled with an asterisk (∗) can be indexed to the new series of reflection peaks of the interlayer of the α-Ni(OH)$_2$.

be obtained: (i) The value of d_{003} ranges from 7.21 to 9.04 Å, and this may be related to the species and amount of anions intercalated in the interlayer of α-Ni(OH)$_2$ too.[20,22a] (ii) Similar to what was presented in Figure 1, the d value of the first diffraction peaks changes from 12.48 to 14.48 Å. which can be regarded as the introduction of an organic molecule in the reaction just like what happened in samples A1−A4.

Altering the reaction temperature did not remarkably affect the d spacings of the end products. If no salts were added to the experimental system, or ammonia or sodium hydroxide solution was selected to replace HMT as the alkali source, no

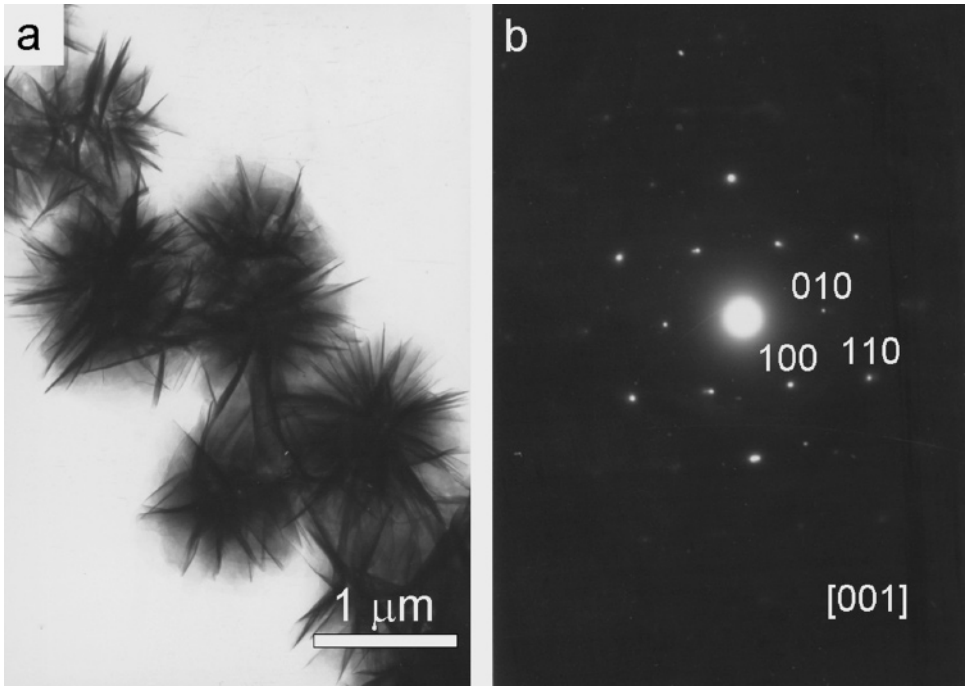

Figure 3. TEM image and electron diffraction pattern of the sample A2 ($Ni(OH)_{1.70}(C_6H_{12}N_4)_{0.10}(Ac^-)_{0.30}(H_2O)_{0.95}$): (a) TEM image; (b) typical electron diffraction pattern taken on on a piece of extended nanosheet of the nanoflower along the [001] direction.

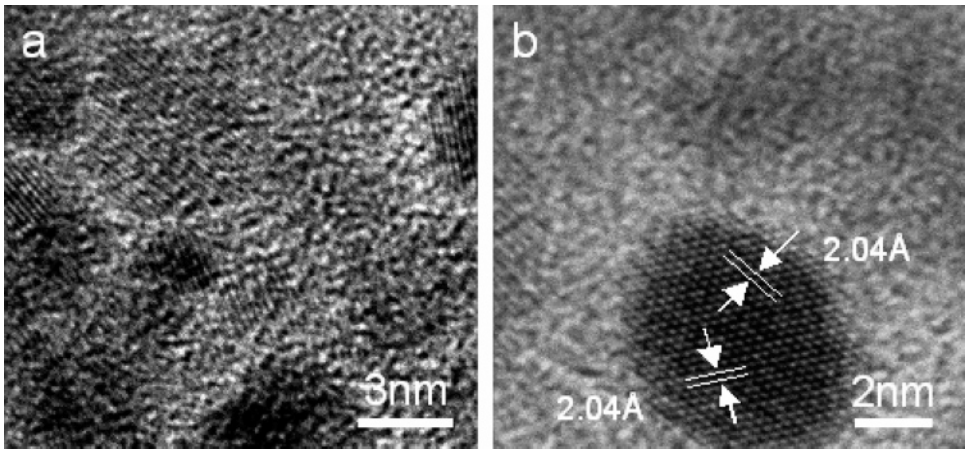

Figure 4. HRTEM images taken on the very thin nanosheets of the flowers shown in Figure 3a after exposure on electron beam for a while: (a) general view; (b) typical Ni nanoparticle formed due to the reduction by the electron beam.

α- nickel hydroxide can form. The effect of anions on the formation of α-$Ni(OH)_2$ is still uncertain at this stage.

Morphology of α-$Ni(OH)_2$ Organic—Inorganic Hybrid Materials. The transmission electron microscope (TEM) image in Figure 3a shows that the sample A2 is composed of flowerlike structures. The electron diffraction pattern taken on on a piece of extended nanosheet of this flower like structure shows a typical single crystalline nature (Figure 3b), which is similar to that hexagonal α-$Ni(OH)_2$ phase (JCPDS Card No. 38-0715). However, the long time exposure of the sample under the electron beam during TEM observation will destroy the structures, accompanied by the formation of a lot of nanoparticles with a size of 3−6 nm (Figure 4a). The lattice-resolved high-resolution TEM (HRTEM) image in Figure 4b showed a spacing of 2.04 Å, corresponding to the value for (111) planes of cubic Ni phase (JCPDS Card No. 04-0850), underlying that the very thin α-$Ni(OH)_2$ nanosheets of the flower structure are not stable under the electron beam and can be reduced into Ni nanoparticles.

The scanning electron microscope (SEM) images of the obtained α-$Ni(OH)_2$ samples are shown in Figure 5. Parts a−d of Figure 5 correspond to the morphologies of the samples A2, B2, C2, and D2 (see the experiment details in Table 1) while the inserted photographs are the enlarged images of each sample. Previous literature reported that α-$Ni(OH)_2$ tended to form a filmlike morphology.[13,22a,35] Recently, hollow spheres and thin films of nickel hydroxide have been fabricated using poly(styrene−methyl acrylic acid) (PSA) latex particles as template.[36] Ribbon- and boardlike nanostructured nickel hydroxide can be synthesized using the amorphous α-$Ni(OH)_2$ as precursor.[37] In this work, flowerlike α-nickel hydroxide nanostructures can be synthesized without using any template. Figure 5 presents the images of various flowerlike morphologies with a diameter ranging from 2 to 10 μm, which are organized by thin α-$Ni(OH)_2$ films with a thickness of about 10 nm. The flower structures shown in Figure 5b,c are more complex and compact than those in Figures 5a,d, while the very thin nanosheets shown in Figures 5a,d are more flexible than those in Figure 5b,c. On

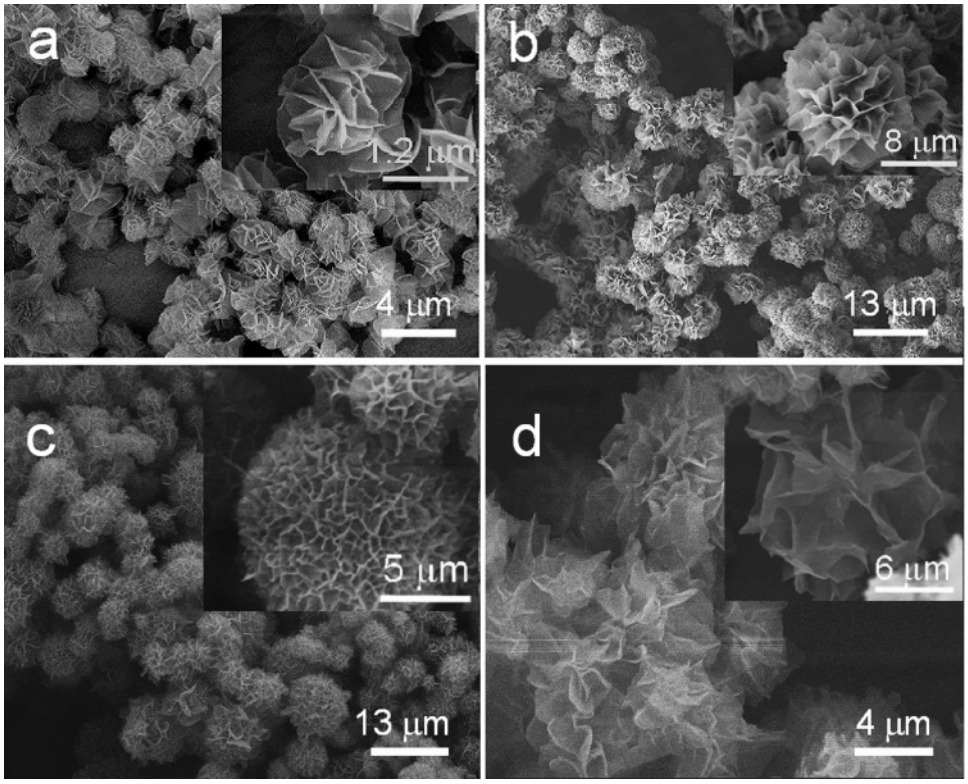

Figure 5. (a−d) SEM images of the α-Ni(OH)$_2$ samples obtained at 140 °C for 10 h for the samples A2, B2, C2, and D2, respectively. The inserted images correspond to the magnified SEM images of these samples.

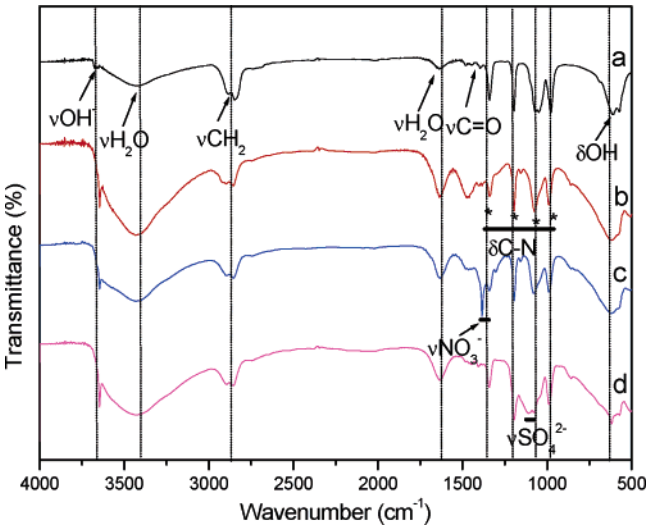

Figure 6. FT-IR spectra of the obtained α-Ni(OH)$_2$ samples: (a−d) samples A2, B2, C2, and D2, respectively.

the basis of these experiments, we can conclude that the reason for this phenomenon is due to various anions in this reaction system, but a more detailed mechanism about the formation of these morphologies is under further exploration.

FT-IR and Thermogravimetric Analysis of α-Ni(OH)$_2$ Organic—Inorganic Hybrid Materials. The Fourier transformation infrared spectra (FT-IR) shown in Figure 6 for the samples A2, B2, C2, and D2 have the same vibration bands at ca. 3650, 3435, 2890, 2850, 1630, 1340, 1195, 1070, 615, and 430 cm^{-1} which are labeled with the dotted lines. The narrow band at ca. 3650 cm^{-1} is attributed to the υ_{O-H} stretching of the geminal free hydroxyl groups of the brucite-like structure,[13,22a] which can be attributed to the flexing vibration of free hydroxyl existed in α-Ni(OH)$_2$ in the samples. A broad band at ca 3435 cm^{-1} is due to the υ_{O-H} vibration of H-bonded water molecules located in the interlamellar space of turbostratic structure of α-Ni(OH)$_2$. The band at ca. 1630 cm^{-1} is characterized to the bending vibrational mode of the interlayer water molecules. The peaks at ca. 2890 and 2885 cm^{-1} are attributed to the −C−H vibrational mode of −CH$_2$−, respectively. The absorption bands at 1020−1220 cm^{-1} are attributed to the vibrational mode of C−N. The band at ca. 615 cm^{-1} is assigned to δ_{O-H} and the band at ca. 430 cm^{-1} can be assigned to metal−oxygen vibrations and metal−oxygen−hydrogen bending vibrations[20,38] that can be ascribed to Ni−OH in this system.

From the FT-IR spectra, we can see that all samples have absorption bands for the −CH$_2$− and C−N functional groups. Furthermore, a weak band at 1400 cm^{-1} in Figure 6a can be indexed to the C═O vibration of CH$_3$COO$^-$. The vibration bands at 1385 cm, 1340, and 830 cm^{-1} in Figure 3c correspond to the vibration of NO$_3^-$ (i.e., an NO$_3^-$ anion with D_{3h} symmetry in the interlayer space)[27] and the vibration band at 990 cm^{-1} in Figure 6d can be assigned to the vibration of SO$_4^{2-}$.[39] Considering the initial materials we used in these experiments, it is believed that a part of the precursor HMT and anions have been intercalated into the α-Ni(OH)$_2$ interlayer.

The element analysis and thermogravimetric analysis (TGA) were used to confirm the above speculation. It is well-known that the α-nickel hydroxide always undergoes multisteps mass loss, and it has a larger mass loss (about 34%) than β-nickel hydroxide (18%). The thermogravimetric curves of the α-Ni(OH)$_2$ (A2, B2, C2, and D2) samples with the temperature ranging from 30 to 600 °C show two steps at ca. 100 °C and ca. 350 °C with different net weight loss, that is 35.2% (A2), 34.1% (B2), 33.1% (C2), and 30.6% (D2), respectively (Figure 7). All the peaks in the XRD patterns in Figure 8 of the end

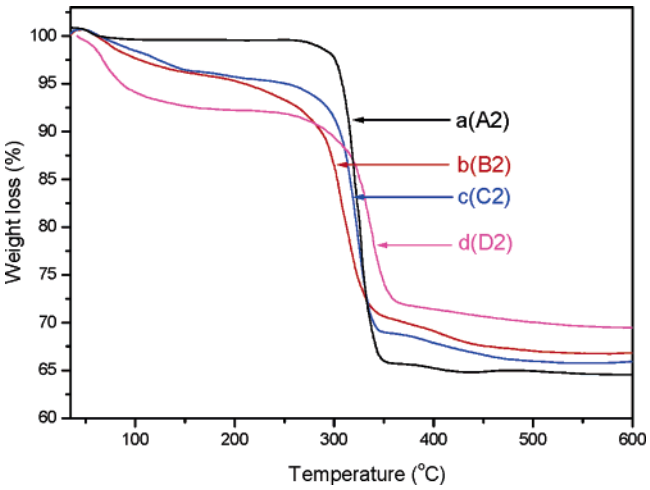

Figure 7. Thermogravimetric curve (TG) of the α-$Ni(OH)_2$ samples: (a−d) samples A2, B2, C2, and D2, respectively.

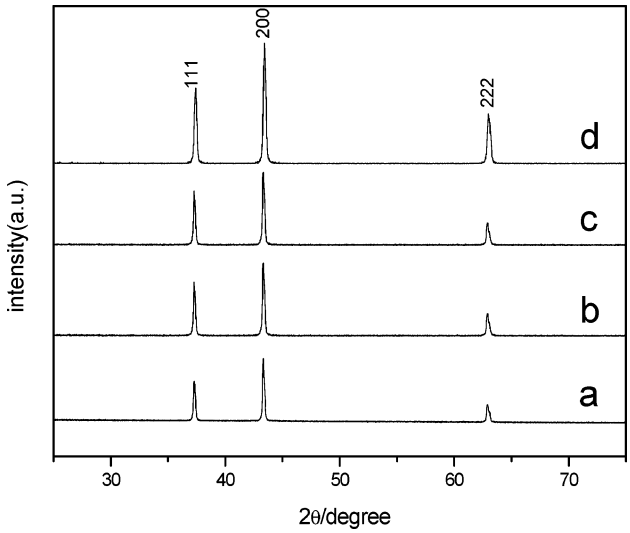

Figure 8. XRD pattern of the NiO products after thermal decomposition of α-$Ni(OH)_2$ samples A2, B2, C2, and D2, respectively.

TABLE 2: Element Analysis Data of Sample A2

element	weight %	atomic %
C	8.63	18.04
N	4.74	8.48
O	30.75	48.20
Ni	47.56	20.32
Cu	8.32	4.96
totals	100.00	

product after TGA measurement can be indexed to the pure cubic NiO with $a = 2.412$ Å (JCPDS 47-1049).

The element analysis data of sample A2 (shown in Table 2) agreed well with those of thermogravimetric analysis, indicating that a small parts of the precursor HMT and anions have indeed been intercalated to the interlayer of α-$Ni(OH)_2$ to form the α-$Ni(OH)_2$ organic−inorganic hybrid materials. On the basis of the results of thermogravimetric analysis and element analysis, the chemical composition of the sample A2 can be formulated as $Ni(OH)_{1.87}(C_6H_{12}N_4)_{0.10}(Ac^-)_{0.13}(H_2O)_{0.37}$. The results of other samples are similar to this and the molecular formulas are listed in Table 3. These results have demonstrated that a new series of α-nickel hydroxide with adjustable interlayer spaces can be synthesized in the present system. The general molecular formula can be summarized as $Ni(OH)_{2-x}(A^{n-})_{x/n}$-$(C_6H_{12}N_4)_y \cdot zH_2O$ (A = Cl^-, CH_3COO^-, SO_4^{2-}, NO_3^-; $x = 0.05-0.18$, $y = 0.09-0.11$, $z = 0.36-0.43$).

TABLE 3: Interlayer Distances and Compositions of the α-$Ni(OH)_2$ Samples with Different Intercalated Anions

sample no.	intercalated anion	interlayer distance (Å)	chemical composition
A2	Ac^-	14.19	$Ni(OH)_{1.87}(C_6H_{12}N_4)_{0.10}(Ac^-)_{0.13}(H_2O)_{0.37}$
B2	Cl^-	13.14	$Ni(OH)_{1.95}(C_6H_{12}N_4)_{0.11}(Cl^-)_{0.05}(H_2O)_{0.36}$
C2	NO_3^-	14.43	$Ni(OH)_{1.82}(C_6H_{12}N_4)_{0.09}(NO_3^-)_{0.18}(H_2O)_{0.40}$
D2	SO_4^{2-}	13.63	$Ni(OH)_{1.78}(C_6H_{12}N_4)_{0.09}(SO_4^{2-})_{0.11}(H_2O)_{0.43}$

Chemical Stability of α-$Ni(OH)_2$ Organic—Inorganic Hybrid Materials. The stability of the synthesized α-$Ni(OH)_2$ samples were investigated by immersing each powder in 6 M HNO_3 and 6 and 12 M KOH solutions for several hours to tens of days. After immersion for a certain period, the products were washed by deionized water and absolute ethanol and then dried at 60 °C for 4 h in a vacuum for powder XRD measurement. The XRD patterns in Figure 9 indicate these products after treatment are also α-$Ni(OH)_2$ which show characteristic diffraction peaks at low angle (2θ is about 10°) around 8.25−10.84 Å and a broad asymmetric band at about 2.66 and 1.54 Å. It was found that the as-synthesized α-$Ni(OH)_2$ (the sample A2) is stable for more than 40 days in 6 M KOH and for more than 48 h in 12 M KOH solution at room temperature. Similar results can be obtained from other samples (B2, C2, and D2) in alkali solutions (data not given).

From the XRD pattern of Figure 9A, it was found that the main diffraction peak for α-$Ni(OH)_2$ samples (curves a−c) which are treated by immersing in strong acid and alkali is shifted to smaller scattering angles compared to that of the primary sample obtained (curve d). On the basis of the reported literature,[40] it is believed that this shift may be induced by ions exchanging; i.e., the hydroxyls have replaced the CH_3COO^- or more water molecules have intercalated into the α-$Ni(OH)_2$ interlayers. This exchangeable progress resulted in enlarging the d values, and the structure of α-$Ni(OH)_2$ layered double hydroxide may be reoriented.[40,41]

To our best knowledge, the chemical stability of α-$Ni(OH)_2$ (the sample A2) in our experiments is better than those of α-$Ni(OH)_2$ materials synthesized by any other method.[13] Interestingly, we found that the α-$Ni(OH)_2$ of the A2 sample can stand erosion of strong oxidant acid (6 M HNO_3) for more than 14 h, but other samples (B2, C2, and D2) failed to tolerate this experimental condition. In comparison with a previous report,[13] we believe that this high stability may be attributed to the species of intercalated organic precursor we used in this experiment. Usually, HMT is a strong chelating ligand with the interaction of transition metal ions; hence, it is reasonable to consider that this high chemical stability is derived from such strong chelating interaction between the Ni ions and HMT molecules. This high stability could make this material more suitable for the applications.

BET Analysis of α-$Ni(OH)_2$ Organic—Inorganic Hybrid Materials. All samples (A2, B2, C2, D2) are determined by N_2 adsorption by BET measurements using an ASAP-2000 surface area analyzer. Among these samples, the sample B2 showed the biggest BET (Brunauer−Emmett−Teller) surface area. N_2 adsorption−desorption isotherm and the pore size distribution curve for the macroporous $Ni(OH)_2$ (the sample B2) are shown in Figure 10. The hysteresis of the desorption branch is due to hindered desorption which is often observed in particulate samples.[42] The pore size distribution calculated from the adsorption branch of isotherm indicated that the $Ni(OH)_2$ retained a relatively uniform framework with pore size distribu-

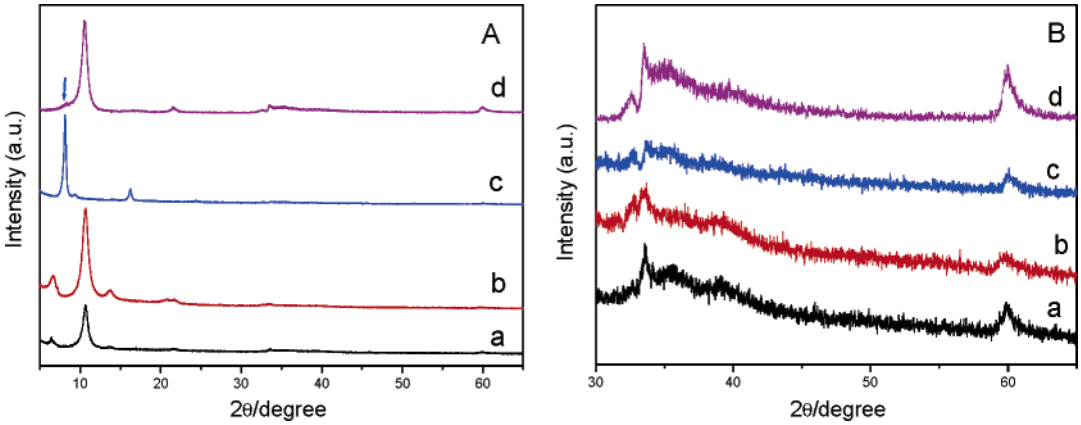

Figure 9. Left (A): XRD patterns taken on the samples after immersing the hydrothermal treatment synthesized sample A2 into the alkali and acidic solutions. Key: the XRD patterns of sample A2 immersed (a) in 6 M KOH for 40 days, (b) in 12 M KOH for 48 h, and (c) in 6 M HNO_3 for 14 h; (d) XRD pattern of the primary obtained $Ni(OH)_2$. (B) is the amplification parts of Figure 9A.

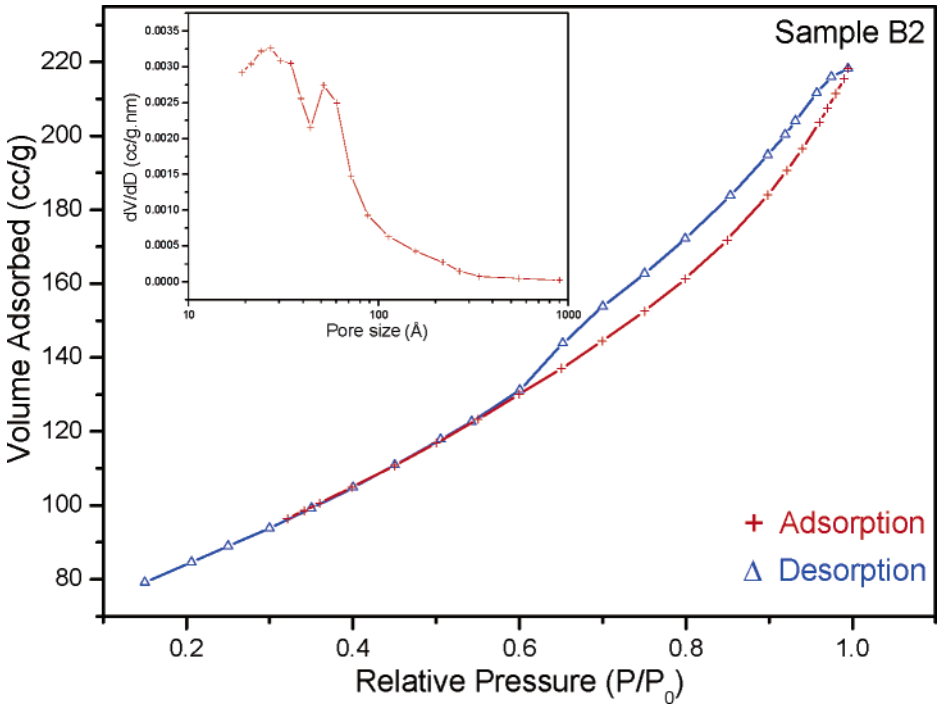

Figure 10. N_2 adsorption−desorption isotherm curve and pore size distribution (inset) of the sample B2.

tion centered at around 50 Å. It is also found that there are micropores existing in the nanosheets of the α-$Ni(OH)_2$ organic−inorganic flowers based on the BET measurement. The micropore area is about 68.03 m^2/g. The BET (Brunauer−Emmett−Teller) surface area, calculated from nitrogen adsorption isotherms, shows that the surface area of the α-$Ni(OH)_2$ sample B2 is 299.26 m^2/g, and the BJH (Barret−Joyner−Halenda) average pore diameter is 45.1 Å. The determined surface area is much larger than that of 62 m^2/g recently reported for the hollow $Ni(OH)_2$ spheres.[36] Similarly, the BET surface areas of other samples are 136.40 m^2/g (A2), 71.22 m^2/g (D2), and 47.08 m^2/g (C2), respectively. From the results of these data, it can be concluded that all the α-$Ni(OH)_2$ organic−inorganic samples synthesized by this approach are of high BET surface area.

Magnetic Properties of α-$Ni(OH)_2$ Organic—Inorganic Hybrid Materials. The magnetic properties of the α-$Ni(OH)_2$ organic−inorganic hybrid materials have been believed to be highly dependent on the shape, crystallinity, magnetization direction, and the *d* spacing of the sample and so on.[43,44] Parts a and b of Figure 11 are the isothermal magnetization loops measured at 4 K on a commercial SQUID magnetometer for the samples B2, C2 with *d* spacings of 13.14 and 14.43 Å, respectively. The hysteresis loops indicated that the samples show a ferromaganetic behavior with saturation magnetization (*Ms*), remanent magnetization (*Mr*), and coercivity (*Hc*) values. The *Hc* values of the sample B2 $[Ni(OH)_{1.95}(C_6H_{12}N_4)_{0.11}(Cl^-)_{0.05}(H_2O)_{0.36}]$ and the sample C2 $[Ni(OH)_{1.82}(C_6H_{12}N_4)_{0.09}(NO_3^-)_{0.18}(H_2O)_{0.40}]$ are 2000 and 1280 Oe, respectively. The different *Hc* for these samples may be ascribed to the different *d* spacings and imperceptible structural difference.[2,44]

Conclusions

In summary, a new family of organic−inorganic hybrid material of α-nickel hydroxide formulated as $Ni(OH)_{2-x}(A^{n-})_{x/n}\cdot(C_6H_{12}N_4)_y\cdot zH_2O$ (A = Cl^-, CH_3COO^-, SO_4^{2-}, NO_3^-, x = 0.05−0.18, y = 0.09−0.11, z = 0.36−0.43) with high chemical stability and adjustable interlayer spacing ranging from 7.21 to 15.12 Å has been successfully prepared by a convenient

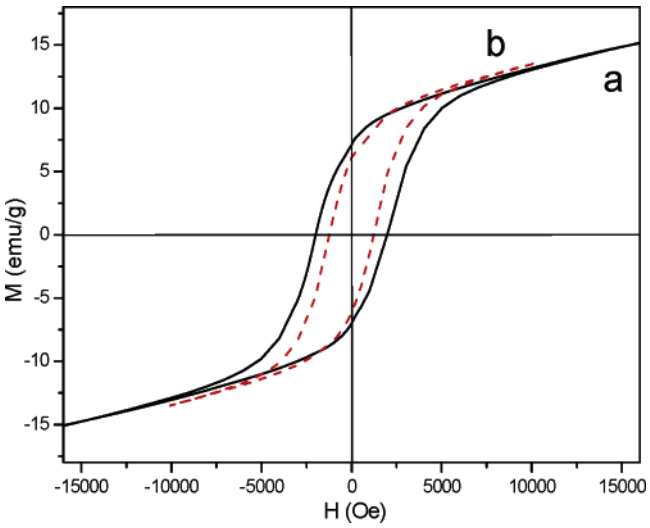

Figure 11. Isothermal magnetization at 4 K for α-$Ni(OH)_2$ samples: (a) isothermal magnetization of the sample B2 (d = 13.14 Å); (b) isothermal magnetization of sample C2 (d = 14.43 Å).

hydrothermal method under mild conditions. The particles are in a form of a flowerlike structure composed of very thin nanosheets. The results demonstrated that different species of anions and dosage of hexamethylenetetramine (HMT) have significant influences on the d spacing value, morphology, magnetic property and surface area of the end product. One of the samples with a formula $Ni(OH)_{1.95}(C_6H_{12}N_4)_{0.11}(Cl^-)_{0.05}(H_2O)_{0.36}$ has a high surface area of about 299.26 m^2/g and an average pore diameter of about 45.1 Å. This family of hybrid materials is of so high stability that they can stand more than 40 days in high alkali solution (6 M KOH) and more than 48 h in 12 M KOH solution at room temperature. Such high stability could be derived from strong chelating interaction between the Ni ions and HMT molecules with the interlayers. This high stability could make this material more suitable for applications. The evaluation of electrochemical properties of this family of hybrid materials is ongoing and will be reported in due course.

Acknowledgment. S.H.Y. would like to express thanks the funding support from the Centurial Program of the Chinese Academy of Sciences, the National Science Foundation of China (Contract Nos. 20325104, 20321101, 50372065), and the Scientific Research Foundation for the Returned Overseas Chinese Scholars supported by the State Education Ministry, the Specialized Research Fund for the Doctoral Program (SRFDP) of Higher Education State Education Ministry, and the Partner-Group of the Chinese Academy of Sciences—the Max Planck Society.

References and Notes

(1) (a) Kunio, O. *Chem. Mater.* **1997**, *9*, 2039. (b) Davis, E. M.; Labo, R. F. *Chem. Mater.* **1992**, *4*, 756.

(2) Mostafa, T.; Souad, A.; Noureddine, J.; Fernand, F.; Philippe, M.; Marc, D. *J. Mater. Chem.* **2002**, *12*, 3238.

(3) (a) Reichle, W. T. *CHEMTECH.* **1986**, *16*, 58. (b) Constantino, V. R.; Pinnavaia, T. J. *Inorg. Chem.* **1995**, *34*, 883.

(4) (a) Ookuba, A.; Ooi, K.; Hayashi, H. *Langmuir* **1993**, *9*, 1418. (b) Kamath, P. V.; Dixit, M. L.; Indira, A. K.; Shukla, V. G.; Kumar, N. *J. Electrochem. Soc.* **1994**, *141*, 1487.

(5) Leroux, F.; Besse, J. P. *Chem. Mater.* **2001**, *13*, 3507.

(6) (a) Taniguchi, A.; Fujioka, N.; Ikoma, M.; Ohta, A. *J. Power Sources* **2001**, *100*, 117. (b) Shukla, A. K.; Venugopalan, S.; Hariprakash, B. *J. Power Sources* **2001**, *100*, 125. (c) Morioka, Y.; Narukawa, S.; Itou, T. *J. Power Sources* **2001**, *100*, 107.

(7) Ovshinsky, S. R.; Fetcenko, M. A.; Ross, J. *Science* **1993**, *260*, 176.

(8) Boschloo, G.; Hagfeldt, A. *J. Phys. Chem. B* **2001**, *105*, 3039.

(9) Oliva, P.; Leonardi, J.; Laurent, J. F.; Delmas, C.; Braconnier, J. J.; Figlarz, M.; Fievet, F. *J. Power Sources* **1982**, *8*, 229.

(10) Kurmoo, M.; Day, P.; Derory, A.; Estournè s, C.; Poinsot, R.; Stead, M. J.; Kepert, C. J. *J. Solid State Chem.* **1999**, *145*, 452.

(11) (a) Portemer, F.; Delahyde-Vidal, A.; Figlarz, M. *J. Electrochem. Soc.* **1992**, *139*, 671. (b) Delahyde-Vidal, A.; Tekaia Ehsissen, K.; Genin, P.; Figlarz, M. *J. Solid State Inorg. Chem.* **1994**, *31*, 823. (c) Kamath, P. V.; Therese, G. H. A.; Gopalakrishnan, J. *J. Solid State Inorg. Chem.* **1997**, *128*, 38.

(12) (a) Cavani, F.; Trifiro, F.; Vaccari, A. *Catal. Today* **1991**, *11*, 173. (b) Reichle, W. T. *Solid State Ionics* **1986**, *22*, 135.

(13) Jeevanandam, P.; Koltypin, Y.; Gedanken, A. *Nano Lett.* **2001**, *1*, 263.

(14) Genin, P.; Delahaye-Vidal, A.; Portemer, F.; Tekaia-Elhsissen, K.; Iglarz, M. F. *Eur. J. Solid State Inorg. Chem.* **1991**, *28*, 505.

(15) Rajamathi, M.; Vishnu, Kamath, P. *J. Power Sources* **1998**, *70*, 118.

(16) Faure, C.; Delmas, C.; Fouassier, M. *J. Power Sources* **1991**, *35*, 279.

(17) (a) Wang, C. Y.; Zhong, S.; Konstantinov, K.; Walter, G.; Liu, H. K. *Solid State Ionics* **2002**, *148*, 503. (b) Dai, J. X.; Li, Sam, F. Y.; Xiao, T. D.; Wang, D. M.; Reisner, D. E. *J. Power Sources* **2000**, *89*, 40. (c) Liu, B.; Wang, X. Y.; Yuan, H. T.; Zhang, Y. S.; Song, D. Y.; Zhou, Z. X. *J. Appl. Electrochem.* **1999**, *29*, 855.

(18) Hu, W. K.; Noréus, D. *Chem. Mater.* **2003**, *15*, 974.

(19) Dixit, M.; Kamath, P. V.; Gopalakrishnan, J.*J. Electrochem. Soc.* **1999**, *146*, 79.

(20) Faure, C.; Delmas, C.; Fouassier, M.; Willmann, P. *J. Power Sources* **1991**, *35*, 249.

(21) Reichle, W. T. *J. Catal.* **1985**, *94*, 547.

(22) (a) Soler-Illia, G. J. D. A.; Jobbágy, M.; Regazzoni, A. E.; Blesa, M. A. *Chem. Mater.* **1999**, *11*, 3140. (b) Avena, M. J.; Vazquez, M. V.; Carbonio, R. E.; de Pauli, C. P.; Macagno, V. A. *J. Appl. Electrochem.* **1994**, *24*, 256.

(23) Ho, K. C.; Jorne, J. *J. Electrochem. Soc.* **1990**, *137*, 149.

(24) Wang, X. Y.; Luo, H.; Parkhutik, P. V.; Millan, A. C.; Matveeva, E. *J. Power Sources* **2003**, *115*, 153.

(25) Braconnier, J. J.; Delmas, C.; Fouassier, M.; Figlarz, M.; Beaudouin, B.; Hagenmuller, P. *Rev. Chim. Mineral.* **1984**, *21*, 496.

(26) Uzunova, E.; Klissurski, D.; Kassabov, S. *J. Mater. Chem.* **1994**, *4*, 153.

(27) Xu, Z. P.; Zeng, H. C. *Chem. Mater.* **1999**, *11*, 67.

(28) Bookin, A. S.; Cherkashin, V. I.; Drits, A. *Clays Clay Mineral.* **1993**, *41*, 558.

(29) Ulibarri, M. A.; Labajos, F. M.; Rives, V.; Trujillano, R.; Kagunya, W.; Jones, W. *Inorg. Chem.* **1994**, *33*, 2592.

(30) Durand-Keklikian, L.; Haq, I.; Matijevic, E. *Colloids Surf. A* **1994**, *92*, 267.

(31) Avena, M. J.; Vázquez, M. V.; Carbonio, R. E.; de Pauli, C. P.; Macagno, V. A. *J. Appl. Electrochem.* **1994**, *24*, 256.

(32) Rouba, S.; Rabu, P.; Ressouche, E.; Regnault, P. L.; Drillon, M. *J. Magn. Magn. Mater.* **1996**, *163*, 365.

(33) Poul, L.; Jouini, N.; Fiévet, F. *Chem. Mater.* **2000**, *12*, 3123.

(34) Faure, C.; Barthomieu, Y.; Delmas, C.; Fouassier, M. *J. Power Sources* **1991**, *36*, 113.

(35) Genin, P.; Delahaye-Vidal, A.; Portemer, F.; Tekaia-Elhsissen, K.; Figlarz, M. *Eur. J. Solid State Inorg. Chem.* **1991**, *28*, 505.

(36) Wang, D. B.; Song, C. X.; Hu, Z. S.; Fu, X. *J. Phys. Chem. B* **2005**, *109*, 1125.

(37) Yang, D. N.; Wang, R. M.; He, M. S.; Zhang, J.; Liu, Z. F. *J. Phys. Chem. B* **2005**, *109*, 7654.

(38) Deabate, S.; Fourgeot, F.; Henn, F. *J. Power Sources* **2000**, *87*, 125.

(39) Frost, R. L.; Weier, M. L.; Kloprogge, J. T. *J. Raman Spectrosc.* **2003**, *34*, 760.

(40) (a) Radha, A. V.; Vishnu Kamath, P.; Shivakumara, C. *Solid State Sci.* **2005**, *7*, 1180. (b) Kloprogge, J. T.; Wildman, J. E. *Am. Mineral.* **2002**, *87*, 623.

(41) Wang, Z.; Lan, T.; Pinnavaia, T. J. *Chem. Mater.* **1996**, *8*, 2200.

(42) (a) Wang, Z.; Heising, J. M.; Clearfield, A. *J. Am. Chem. Soc.* **2003**, *125*, 10375. (b) Subbia, A.; Pyle, D.; Rowland, A.; Huang, J.; Narayanan, R. A.; Thiyagarajan, P.; Zon, J.; Clearfield, A. *J. Am. Chem. Soc.* **2005**, *127*, 10826.

(43) Murielle, G.; Mireille, R.; Serge, V. *J. Mater. Chem.* **2002**, *12*, 851.

(44) Richard-Plouet, M.; Vilminot, S. *J. Mater. Chem.* **1998**, *8*, 131.